# Estimating surface velocities from satellite data and numerical models: implementation and testing of a new simple method

Alessandro Mercatini[a], Annalisa Griffa[a,b], Leonid Piterbarg[c], Enrico Zambianchi[*,d], Marcello G. Magaldi[b]

[a] *CNR, ISMAR, La Spezia, Italy*
[b] *RSMAS, University of Miami, USA*
[c] *University of Southern California, USA*
[d] *DiSAm, Università Parthenope, Napoli, Italy*

**Abstract**

A simple method of fusing tracer observations and model outputs for computing surface velocities in the ocean is implemented and tested in the framework of the twin experiment approach. Synthetic data from realistic velocity outputs produced by the operational Mediterranean Forecasting System (MFS) are used. The method (Piterbarg, 2009) allows to estimate a velocity field using two consecutive tracer snapshots. The focus is on testing realistic time intervals between snapshots and partial tracer observations. The considered configuration consists of a tracer patch released and advected by the current, and is motivated by the practical problem of estimating velocities and concentrations using satellite data in case of pollutant releases such as oil spills. An extensive set of experiments has been carried out, and the method performance has been quantified in terms of improvements in accuracy with respect to the model. The improvement ranges from values of approximately

*Corresponding author

80-90% for concentration and 50-60% for velocity in the case of almost perfect data, to values of 30-40% for realistic time intervals of the order of days and reduced tracer information, and values of 15-20% when only the boundary of the patch is observed. The results are found to be robust to flow variability and patch parameters.
*Key words:* remote sensing, oil spills, transport processes, tracers, mathematical models, ocean circulation
Mediterranean Sea, Ligurian Sea

---

## 1. Introduction

The problem of estimating velocities from tracer information has a long history in physical oceanography. Earlier works focused on how to obtain estimates of the large scale circulation from in-situ hydrographic vertical sections. Computing relative geostrophic velocities (or velocity vertical shear) from hydrostatic data is quite straightforward, but computing the absolute value of velocity is very challenging, since it is an underdetermined problem. In the 1970's two revolutionary methods were proposed to attack this problem: the "beta spiral" method by Stommel and Schott (1977) and the "inverse" method by Wunsch (1977, 1978). Even though the methods are different, they are conceptually related. Potential density surfaces are considered as material surfaces, so that conservation of potential vorticity and possibly other tracers provide additional constraints that allow to determine the absolute velocity. Building on these pioneering works, a number of methods has been proposed and used in the literature, based on potential vorticity balance (Olbers et al, 1985), on the Bernoulli theorem (Needler, 1985) and

on generalized applications of the concept of Ertel's potential vorticity (e.g. Haynes and McIntyre, 1990; Marshall et al., 1993; Kurgansky et al, 2002)

In the last two decades, information on tracer distribution at the ocean surface has hugely increased thanks to the availability of several different sensors carried by various satellites. Their resolution goes from hundreds of meters to kilometers, allowing to resolve mesoscale phenomena. Even though satellite data have limitations, such as cloud coverage inhibiting the observation of the sea surface at certain wavelengths, they provide a wealth of information which has prompted the development of new methods to optimize their use. Estimating surface velocities from satellite measurements is conceptually different from using in-situ vertical tracer sections. Estimation methods essentially rely on the use of image sequences where the tracer (or its proxy) is assumed to be transported by the currents and to obey a known equation such as the advection-diffusion equation in two dimensions. The main challenge is represented by the fact that while the cross-gradient velocity information can be retrieved from the tracer distribution at subsequent times, the along-gradient component cannot be directly inferred. The problem can be looked at as a classical inverse problem applied to the tracer equation (Fiadeiro and Veronis, 1984; Kelly, 1989).

Various approaches to tackle this problem have been proposed in the literature. Under the assumption of stochastic forcing, the problem can be formulated as a statistical estimation of unknown parameters (Frankignoul and Reynolds, 1983; Ostrovskii and Piterbarg, 1995; 1997; 2000). This approach, even though general and powerful, is based on the assumption of slowly varying fields and therefore cannot be effectively applied to mesoscale

velocities. Significant efforts have also been focused on methods that project the surface velocity on the gradient of the remotely observed field, and use various constraints or regularizations to reconstruct the two-component velocity field (Cohen and Herlin, 1996; Memin and Perez, 1998; Bereziat et al., 2000; Vigan et al., 2000; Corpetti et al., 2002; Isambert et al., 2005). The Maximum Cross Correlation method (MCC) is also worthy of mention, a procedure that is not based on the inverse approach and is applicable when image time series at high temporal resolution are available (Emery et al, 1986; Emery et al., 1992; Crocker et al. 2007). Finally, we would like to mention a recent method based on tracking singularities in the tracer field (Turiel et al. 2008) which very accurately detects mesoscale flow features, although it is not able to estimate the velocity magnitude.

Another avenue that is expected to become more prevalent as ocean circulation models progressively gain in resolution and predictive skills is to use assimilation techniques to combine information from satellite data with information from the circulation models describing the evolution of the velocity field (Bennett, 1992). Some first steps in this direction have been recently proposed (Herlin et al., 2004; Cuzol and Memin, 2005; Papadakis et al., 2005; Herlin et al., 2006; Huot et al., 2006; Korotaev et al, 2008), at least for simplified dynamical models for the velocity. Generalizations to more realistic circulation models are possible, but they require significant technical development and could lead to possible problems of incompatibility between model velocities and satellite data in terms of dynamics and/or resolution.

Conceptually, these approaches are similar to those applied to surface Lagrangian data for the reconstruction and assimilation of the velocity field

(Molcard et al., 2003; Taillandier et al., 2008). Lagrangian data provide information on the fluid particle positions at discrete time intervals, and consecutive observations can be used to estimate the velocity, provided that the time interval is smaller than the typical Lagrangian time scale $T_L$, (i.e. the time over which particle velocity is self-correlated; $T_L$ for the surface ocean typically varies in the range $1 - 5$ days, see e.g. Bauer et al., 2002; LaCasce, 2008; for the Mediterranean see Falco et al., 2000; Poulain and Zambianchi, 2007). The simplest methods estimate the velocity as the ratio between position and time increments (e.g. Hernandez et al., 1995), while more general and powerful approaches introduce an appropriate observational operator based on the particle advection equation, and correct the Eulerian velocity field requiring a minimization of the difference between observed and modeled trajectories (Molcard et al., 2003; Taillandier et al., 2006a; Ide et al., 2002; Salman et al., 2006).

Even though conceptually similar, tracer observations are more challenging than Lagrangian data because tracer particles are not individually tracked: rather, only the gradients of the tracer are observed. As a consequence, only information on the cross-gradient velocity can be directly extracted from successive tracer observations. Approaches based on appropriate observational operators are possible also for tracer data, but they need more extended sequences of successive measurements or additional information in order to constrain the along-gradient velocity (Korotaev et al., 2008).

In this paper we consider a method for tracer data that has been recently proposed by Piterbarg (2009). The method, that is based on only two successive snapshots of the tracer distribution combined with model infor-

mation, can be considered as a first step toward a full assimilation approach. Actual assimilation implies that the dynamical model that generates the velocity field is corrected using the data. In the cited paper, instead, model velocity outputs are used together with satellite data to obtain an optimized "blended" velocity, while the actual evolution of the velocity model is not altered. The blending is performed using a fuzzy logic approach, and the information from the model is used to remove the uncertainty of the along-gradient velocity. The method is general and includes a tracer equation with sources and sinks in addition to the basic advection and diffusion. In the simplest case, when sources and sinks are zero or assumed known, the along-gradient velocity simply coincides with the model estimate.

While the use of full assimilation is expected to provide more complete corrections, the present method has the advantage of being very simple and portable. By combining model outputs and satellite data it can be easily used for any dynamical model and in particular for complex operational ones. The method is therefore especially promising for practical applications where for example real-time corrections of the velocity field are necessary to improve the prediction of the spreading of the pollutant.

The method is tested using synthetic information from a realistic operational model in the Mediterranean Sea, implemented in the framework of the Mediterranean Forecast System (MFS). We use the classical "twin experiment" approach (Molcard et al., 2003; Taillandier and Griffa, 2006) where a main control run is regarded as the "true" ocean, and a tracer is released at its surface and advected. Another run, starting from a different initial condition, is regarded as the "model", reflecting our incomplete knowledge

of the true ocean. The tracer is "observed" in the truth at time intervals $\Delta t_{obs}$, and the surface velocity is estimated combining the tracer data and the model outputs. The method skills are evaluated through a quantitative comparison with the control velocity field.

The specific configuration that we consider consists in releasing a localized tracer patch and advecting it in the flow field. The configuration is motivated by the practical application of a pollutant released from a source, such for instance an oil spill, observed by visible, infrared or microwave satellite sensors. An extensive sensitivity study is performed, varying the interval $\Delta t_{obs}$ between successive observations in a realistic manner, and considering degradation in the quality of the data going from idealized perfect data to reduced data describing only the patch boundary. Also the time and space variability of the applications, and the dependence on the parameters of the patch are considered.

The paper is structured as follows. In Section 2, a brief description of the method is provided, while the experimental setup is described in Section 3. Results are presented in Section 4 and a summary and concluding remarks are given in Section 5.

## 2. The method

### *2.1. Problem statement*

We start with a description of the general setup and will proceed to specifying the goals for the present work. First, let us assume that the normalized concentration $c(x, y, t)$ of a tracer is known from successive satellite observa-

tions and its evolution is described by the following transport equation

$$\frac{\partial c}{\partial t} + u\frac{\partial c}{\partial x} + v\frac{\partial c}{\partial y} = f(x, y, t) \tag{1}$$

where $x, y$ are the two-dimensional (horizontal) surface coordinates and $t$ is time, $u, v$ are the two Cartesian components of the surface velocity $\mathbf{u}$, and $f$ represents the sum of all the source and sink processes acting on the tracer.

Notice that in the case of an oil spill application, $f$ includes a source term describing the pollutant release, the dissipation due to turbulent motions and all the "fate" processes describing the chemical transformations of the oil patch. The advection velocity $\mathbf{u}$ includes not only the ocean currents but also the wind component that contributes to advect the spill at the ocean surface. In the following applications (Section 3 and 4) the wind component is not explicitly considered, but the methodology would not change if it were included.

Thus, for a fixed point in space and time (1) represents a straight line

$$Au + Bv + E = 0 \tag{2}$$

in the $(u, v)$ plane with

$$A = \frac{\partial c}{\partial x}, \quad B = \frac{\partial c}{\partial y}, \quad E = \frac{\partial c}{\partial t} - f \tag{3}$$

Now, let us suppose that the forcing $f$ is not known exactly, but rather some bounds are available; in particular, let $f_b$ be a first guess (background) value of $f$ estimated from satellite observations (or, for the sake of generality, from any other data source), with a precision $h$, i.e.

$$|f - f_b| < h \tag{4}$$

The consequence of (4) in the $(u, v)$ plane is represented by a confidence region for the unknown velocity $\mathbf{u}$, shown in the left panel of Fig. 1 as a shaded strip.

Finally, let us assume that velocity outputs $\mathbf{u}_m$ from a circulation model are available, providing estimates of the surface velocity, as shown by the red points in Fig.1. The problem is to aggregate the above information to get an optimal estimate $\mathbf{u}_{est}$ of $\mathbf{u}$.

A procedure realizing such a goal is commonly called data/model fusion, to be distinguished from traditional assimilation where an estimate is obtained iteratively by injecting observations along the model run time.

*2.2. Fuzzy logic approach and particular application*

The above problem is a good target for methods based on the fuzzy set theory (on fuzzy logic see, e.g., Dubois et al, 1997) since the boundaries of the confidence regions for data and model are quite vague and no statistical approach is possible because of small samples. Such a method was developed by Piterbarg (2009) and tested on idealistic flows, the general case of unknown but bounded forcing (4) was considered, and the method was tested in the ideal case of perfect tracer observations and small observation time interval $\Delta t_{obs}$, allowing a faultless computing of the tracer time derivative.

In fuzzy logic uncertainties are parametrized by means of membership functions, rather than using probability distributions and other statistical characteristics which are difficult to estimate from poor samples, as is typical in the case of ocean observations. A membership function $m(x)$ for a fuzzy variable $X$ takes values between 0 and 1. In particular, $m(x) = 1$ if $x$ is a possible value of $X$ and $m(x) = 0$ if $x$ is an impossible value. If for

some value $x$ our knowledge is not enough to assign it to either category, then $0 < m(x) < 1$. As to the velocity estimation problem, a membership function $m_o(u, v)$ for the unknown velocity coming from observations is set to be 1 if $|Au + Bv + E_b| < h$, 0 if $|Au + Bv + E_b| > h'$, and to be between 0 and 1 otherwise, where $E_b = \frac{\partial c}{\partial t} - f_b$ and $h'$ is a limit that the deviation $|f - f_b|$ will never exceed while $h$ is just a reasonable estimate for this deviation. Similarly, another membership function $m_b(u, v)$ can be defined, on the basis of model experiments. One of the most widespread methods of deriving a point estimator from an aggregated membership function (what in the fuzzy logic context is called defuzzification) is to take $\mathbf{u}_{est}$ as the centroid of the region described by the function $f(u, v) = min\{m_o(u, v), m_b(u, v)\}$. This is indeed the algorithm used in Piterbarg (2009) with some further simplifications.

Thus, the only assumption for the fuzzy logic algorithm is an approximate knowledge of the range for the unknown RHS in the transport equation and of the range of variabilty of the model velocity estimates.

In the present paper, the method is tested focusing on the problem of realistic $\Delta t_{obs}$ and reduced tracer observations, while restricting ourselves to the case of known forcing $f$. In the case of known $f$ the confidence strip degenerates into a straight line given by (2) and the general solution suggested by Piterbarg (2009) reduces to orthogonal projecting the model output onto this line (Fig.1, right panel). The corresponding estimation formulas become straightforward:

$$u_{est} = u_m - \frac{A(Au_m + Bv_m + E)}{A^2 + B^2}, \quad v_{est} = v_m - \frac{B(Au_m + Bv_m + E)}{A^2 + B^2} \qquad (5)$$

allowing at the same time a very clear interpretation. Let us comment on

(5) which will represent the main tool in the experiments described in the following.

First, equations (5) can be equivalently obtained by setting the component of $\mathbf{u}_{est}$ orthogonal to tracer lines equal to that computed from the tracer observations only and setting the tangent component equal to the model one. The latter is quite logical since no information on this component can be derived from the tracer (e.g., Fiadeiro and Veronis, 1984).

Second, the proposed estimate always improves the first guess as can be seen from Fig.1 (right panel). Indeed the true velocity lies on the indicated straight line and the model error is represented by the length of the hypotenuse while the estimation error is the length of a leg. Moreover, in Piterbarg (2009) it is shown that on average the relative improvement with respect to the first guess has a lower bound of $1 - 1/\sqrt{2}$, i.e. about 30%

Then, it can be checked from (5) that

$$Au_{est} + Bv_{est} + E = 0 \tag{6}$$

i.e. the estimated velocity field transfers the tracer in the same way as the true velocity does, a very important property when using the estimate for predicting the tracer spreading (practically, however, (6) holds only approximately, with an unknown error because of space/time discretization).

Finally, computational procedures based on (5) are extremely fast and stable.

On the other hand, one of the drawbacks of the suggested method is that it is a pointwise procedure which sometimes leads to a somewhat irregular field estimate requiring a spatial smoothing.

## 3. Experimental setup

### *3.1. Numerical implementation*

The method is implemented and tested using synthetic data in the framework of the twin experiment approach. The case of a purely advective tracer is considered, so that the source/fate term $f(x, y, t)$ in (1) and (3) is set equal to zero in the numerical simulations. Notice that the results can be easily generalized to the case of an exactly known function $f(x, y, t)$ as discussed in Section 2, while the effects of a partially unknown $f(x, y, t)$ can be significantly different (Piterbarg, 2009), and they will be addressed in future works considering specific applications.

In the present implementation, the velocity fields are provided by the outputs of the operational Mediterranean Forecasting System (MFS) in the northwestern Ligurian Sea (Fig. 2). A similar setup has been already used in one of the test cases in Piterbarg (2009) to illustrate the method considering the ideal case of complete tracer information. Here a more systematic investigation of realistic observation parameters is carried out. The MFS ocean model is a discretized version of the primitive equations based on the OPA model and implemented on the Mediterranean basin. The configuration is the one described in Tonani et al. (2008), generated over a meshgrid of resolution $\Delta s$= 1/16 degree (i.e. approximately 6 km). The MFS observing system includes sea surface topography and temperature and salinity profiles, routinely assimilated in the model. Background error correlations are computed with vertical time-dependent EOFs as reported in Dobricic et al. (2005).

In our twin experiment the MFS control run (Truth) consists of a sequence

of daily average velocities, $\mathbf{u}$, starting at a given day IT1. A tracer is released at IT1 and advected during the following 3 days. The tracer has an initial Gaussian shape with width (standard deviation) $R$, simulating the released patch. The tracer distribution is observed at time intervals $\Delta t_{obs}$, stored and considered as representative of the True satellite data. The Model run, which provides $\mathbf{u}_m$, consists of MFS model daily average outputs from a different initial state, IT2, corresponding to three days after IT1. The tracer data extracted from the Truth are used at each interval $\Delta t_{obs}$ to correct the Model velocity using equations (3) and (5), and producing the Estimate velocity fields $\mathbf{u}_{est}$. Model and Estimate velocity fields $\mathbf{u}_m$ and $\mathbf{u}_{est}$ are also utilized to advect the tracer, using the same initial deployment conditions of the Truth run, thus providing Model and Estimate tracer concentration fields, $c_m(x, y, t)$ and $c_{est}(x, y, t)$ respectively, which can be compared with the True tracer concentration.

The method performance is quantitatively assessed considering the differences between the velocity and the tracer fields of Estimate and Truth, and quantifying the improvements with respect to the Model. The quantitative metrics describing the Estimate error ($Er$) and gain ($Gain$) are defined as follows and applied to both the velocity and tracer estimates:

$$Er = \frac{rms(Estimate - Truth)}{rms(Model - Truth)} \tag{7}$$

$$Gain = \frac{rms(Model - Truth) - rms(Estimate - Truth)}{rsms(Model - Truth)} = 1 - Er \tag{8}$$

where $rms$ is the root mean square.

From the numerical point of view, the advection equation (1) is discretized

using a third order upwind method (Durran, 1999) with open boundary conditions (Kantha and Clayson, 2000). The scheme has been chosen as a good compromise between stability, accuracy and numerical simplicity. A certain degree of numerical diffusion is expected to exist, but this is not a problem for the present applications. Our goal is not to provide a perfect simulation of a pure advection process but rather to consider a realistic application, where deviations from perfect advection are expected to occur. The numerical diffusion can be considered as mimicking the effects of environmental small scale diffusion that are not resolved by the model.

The estimations (3) and (5) are performed computing finite difference approximations of the derivatives $A, B, E$ from the tracer data. A central finite difference operator is used for the space derivatives and an upwind operator for the time derivative. After applying (5), the velocity estimate is smoothed to avoid noise at the grid scale using a simple Gaussian kernel with a standard deviation corresponding to 2 grid points.

*3.2. Region of application and flow parameters*

The region of interest is the Ligurian Sea, a sub-basin of the Mediterranean Sea characterized by a general cyclonic circulation and by the presence of a number of mesoscale recirculating gyres especially in the summer (Astraldi et al., 1990). Two recent experiments have been performed in the Ligurian Sea, MREA07 and MREA08, and the MFS model is presently being validated on the basis of those data (Fabbroni et al., 2009 a,b). The specific domain of application is shown in Fig.2 and has a size of $21 \times 17$ grid points.

The region is located in the northern Mediterranean Sea, in the same general area previously considered by Taillandier et al. (2006b) in their

study on velocity reconstruction using Lagrangian data. Typical space and time scales of the velocity field, as shown by the OPA model solutions and confirmed by observations, are discussed in Taillandier et al. (2006b), and are summarized in the following as they are relevant to the applications of the present method. The mesoscale structures have space scales ranging from $R_E \approx 10$ km for the smaller recirculating structures to $R_E \approx 30$ km for the main cyclonic gyre. The typical mesoscale time scale $T_E$, evaluated as the e-folding of the velocity autocorrelations at fixed grid points, is of the order of 10 days or more. Superimposed to this there is a clear high frequency inertial signal with $T_I \approx 17$ h. The Lagrangian time scale $T_L$, computed from the velocity autocorrelation following trajectories, is significantly shorter than $T_E$: $T_L \approx 3$ days. Overall, the field is characterized by $T_I < T_L < T_E$, a typical condition for mid-latitude flows in the open ocean or in regional seas (e.g. Lumpkin et al., 2002).

In the present application, we concentrate on the mesoscale and larger components of the flow, as reflected by the fact that we consistently use daily average velocities for Truth and Model velocity, therefore removing the effects of higher inertial frequencies. A conceptually similar approach, focused on mesoscale, has been followed also in Taillandier et al. (2006b, 2008). Estimation of higher frequencies and/or smaller scale motion is expected to require a very large amount of data, and also the models are expected to be unreliable at those scales due to limitations in small-scale forcing knowledge, resolution and parameterization. The most important time scale in our applications is expected to be $T_L$, especially in relation to the size of the interval $\Delta t_{obs}$ between observations. We can expect that for $\Delta t_{obs} > T_L$ the information on

velocity from tracer advection is significantly reduced, similarly to the case of Lagrangian data. In the applications discussed in this paper we consider a range of $\Delta t_{obs}$ up to 3 days, i.e. $\Delta t_{obs} \leq T_L$. We anticipate, though, that as shown by the results in Section 4 and differently from the Lagrangian data case, the velocity estimation poses additional stability constraints on $\Delta t_{obs}$, depending also on the size of the space discretization $\Delta s$.

As to the spatial scales of the observations, we can expect that in order to efficiently correct the mesoscale, the tracer configuration must have main gradients at scales comparable to (or smaller than) the mesoscale. In the present experiments, suggested by the specific application for oil spill prediction observations, the size of the patch (typically smaller than the mesoscale structures) corresponds to the size of the gradient and therefore controls the correction. For different applications, such as for instance for sea surface temperature or ocean color observations, where the tracer covers the whole domain, the effectiveness of the correction will depend on the size and location of the main gradients in each realization.

### *3.3. Numerical experiments and parameter sensitivity*

A series of experiments, for a total of approximately 100 cases, has been performed to test the skill of the estimation method varying a number of parameters (summarized in Table 1).

The first set of experiments, called BASE experiments, tests the sensitivity to the main observation parameters, i.e. the interval between observations $\Delta t_{obs}$ and the type of tracer information available (as defined in the following). In this series of experiments the velocity is assumed to be constant in time for 3 days for simplicity, and corresponds to the MFS output with IT1=

May 26 2007 for the Truth and IT2 = May 29 2007 for the Model. In all the experiments, the same release location $\mathbf{x}_0$ is considered, corresponding to the grid point (15,8), and an initial Gaussian tracer distribution with $R = 2\Delta s$ is used. In the BASE experiments, the observation parameters are varied in the following way. A range of values for $\Delta t_{obs}$ is considered, going from idealized values of the order of a quarter of an hour to realistic values for satellite observations of the order of few days. The method is implemented in the most straightforward way, i.e. applying it independently to each sequence of successive measurements, without imposing any form of persistency to the correction. As to the spatial extension of tracer information, three different modalities are considered, chosen so as to encompass different tracer distribution data possibly available from satellite observations. An ideal case is considered first and indicated as modality $CA$, where the exact values of the concentration throughout the region of interest are assumed known. We recall that the patch has a Gaussian shape, so that even though most of the tracer is concentrated within the width R, non-zero concentration is actually found throughout the domain. The information is then degraded to the modality indicated as $CC$, where the concentration is known only inside the patch, defined by a cutoff value of the concentration $c_{cutoff}$ ($c_{cutoff}$=0.1 for the BASE experiments). Finally, the most realistic modality is considered where only the boundary of the patch is observed, indicated as $CB$. In this case, the observed concentration is assumed to be zero outside from the patch and constant in the interior.

A second and wider set of experiments, VAR (partly overlapping BASE for two cases), has been run to test the robustness of the estimation results

in terms of spatial and temporal variability of the flow field. A matrix of 10 release locations in the region of interest has been considered (Fig.3), and two different realizations of the velocity field. The first one is the same as in BASE, while the second one considers a sequence of 3 successive daily outputs from the MFS model starting from the same days as in BASE. In all the estimations, the initial patch has the same width as in BASE, $R = 2\Delta s$, and the estimation is performed for $CC$ and $CB$ considering the realistic value $\Delta t_{obs} = 1$ and again $c_{cutoff}$=0.1.

Finally, a last set of experiments, PATCH, explores the sensitivity to the patch parameters R and $c_{cutoff}$, and to its propagation dynamics which is affected by different degrees of numerical diffusivity. All the other parameters are kept as in BASE.

## 4. Results

### *4.1. The BASE experiments: sensitivity to observation parameters*

Fig. 4 shows, as an example, the results of one of the BASE experiments in terms of reconstruction of the tracer and of the velocity fields: the upper panels show the Truth velocity field and the tracer patch as advected by the Truth velocity field; the upper-middle panels depict the Model velocity field and the tracer patch as advected by the latter. It is worth noticing that both Truth and Model velocity fields show the presence of a main cyclone, but the specific characteristics of the flow are different in the two realizations, resulting in significantly different tracer concentrations after 3 days due to the cumulative effect of advection. The lower-middle and lower panels show the velocity field as reconstructed by the method and the tracer field resulting

from its advection, for the modality $CA$ and with $\Delta t_{obs} = 0.1$ days (lower-middle) and $\Delta t_{obs} = 0.25$ days (lower).

The main results of the BASE experiments are summarized in Fig.5, where the $Gain$ for the estimates of velocity (upper panel) and concentration (lower panel) are shown versus $\Delta t_{obs}$ and for the three different modalities of observations $CA$, $CC$, $CB$ (blue, red and green lines respectively). The $Gain$ is computed at day 3 using the metric (8), calculated in the area where the correction is most active, i.e. inside the patch, where the concentration is significantly different from zero and greater than the cutoff value $c_{cutoff}$. A number of preliminary tests has been performed computing the $Gain$ over the whole region, i.e. without cutoff, and they have shown that while the values are consistent, the $Gain$ computed with the cutoff is generally less sensitive to the details of the realization and shows more clearly the dependence on the main parameters such as $\Delta t_{obs}$. Notice that, since the velocity is estimated but not assimilated in the operational model, each correction at every $\Delta t_{obs}$ is independent from the previous ones and the values of $Gain$ keep approximately constant during the three day experiments. The concentration, on the other hand, is integrated over $\mathbf{u}_{est}$, and the value of $Gain$ at day 3 depends on the evolution during the previous days.

The general behaviour of the $Gain$ in Fig.5 shows that the estimation skills decrease as the information deteriorate, i.e. at increasing $\Delta t_{obs}$ and going from $CA$ to $CB$, as can be expected. The specific characteristics of this general trend, though, are not trivial and they are discussed in detail in the following.

The highest $Gain$ values are obtained for $CA$, i.e. for complete informa-

tion on the concentration (blue lines in Fig.5), reaching values of 80%-90% for the concentration and 50%-60% for the velocity. These values are close to the theoretical values for the estimates (3) and (5), obtained when the cross-gradient velocity is perfectly estimated from perfect observations in space and time (Piterbarg, 2009). In this case, the concentration *Gain* is expected to reach 100%, while the velocity gain (defined in terms of both velocity components) is expected to be of the order of 30% or more, depending on the cross-gradient correction in the specific realization. Notice that the maximum values of the *Gain* for $CA$ are obtained for $\Delta t_{obs} \approx 0.2$ days. Examples of the estimated velocity $\mathbf{u}_{est}$, and tracer $c_{est}$ at day 3 for $\Delta t_{obs}$ =0.1 and 0.25 days respectively are shown in Fig.4 (lower panels). In both cases the method appears to effectively correct the fields, as shown by the closer resemblance to the Truth than to the Model (upper panels), but the results appear significantly better for $\Delta t_{obs}$ =0.1 days, as appears especially in the concentration patterns.

For values of $\Delta t_{obs} > 0.25$ days, the *Gain* values for $CA$ are not reported in Fig.5 because the method does not converge and provides overflow values. This can be explained in the following way. Let us consider first the (forward) advection equation (1) and recall that its integration is stable only if the CFL criterion holds (Courant et al., 1928), i.e. $U\Delta t/\Delta s < 1$, where $U$ is a typical value of velocity and $\Delta t$ is the numerical time step. In our case, assuming $U$ =20 cm/s, $\Delta t$ must be $\Delta t < 0.3$ days for the CFL criterion to hold. In all the forward integrations of (1), the numerical $\Delta t$ is kept at $\Delta t = 0.01$ days, so that the criterion always holds. Outside the patch, however, where the tracer concentration is low and the gradient weak, the tracer field evolution may

show Gibbs oscillations due to the advection scheme utilized. On the other hand the estimation formulas (3) and (5) are also based on the discretization of the advection terms, but in this case the relevant time interval is not the numerical $\Delta t$ interval, but rather the interval between observations $\Delta t_{obs}$ used to estimate the derivatives. It can therefore be expected that when $\Delta t_{obs}$ gets close to the CFL limit, the advective signal is not correctly resolved. This is especially true in the regions outside the patch where the tracer concentration is very low and numerical oscillations are present with spatial scales of the order of the grid size. These conditions can cause overflows in an estimation method which is based on the spatial derivatives of the concentration. In our experiments the overflows are indeed observed only in the $CA$ case, as this is the only case where the tracer distribution over the whole domain is used, thus including those regions characterized by very low tracer concentration.

The *Gain* for $CC$, i.e. for information limited to the concentration inside the patch, is shown by the red lines in Fig.5. The curves show a behaviour qualitatively similar to the one for $CA$ (blue lines) for small $\Delta t_{obs}$, with maximum values slightly lower, as can be expected given that the information is degraded with respect to that case. As expected from the above discussion, for $\Delta t_{obs} > 0.25$ days, the overflow occurred for $CA$ does not happen for $CC$, and the *Gain* tends to progressively decrease at increasing $\Delta t_{obs}$. For realistic $\Delta t_{obs}$ for satellite data (of the order of 1-2 days), the *Gain* is of the order of 40-50% for the concentration and 25-35% for the velocity.

Finally, the *Gain* for $CB$, i.e. for data on the patch boundary only, is depicted by the green lines in Fig.5. Its dependence for the concentration on $\Delta t_{obs}$ is even weaker than for $CC$, while for the velocity the *Gain* appears

quite low for small $\Delta t_{obs}$, reaching its maximum at around 0.2 days. This is likely due to the fact that the spatial information is degraded (and reduced to one gradient only, along the boundary of the patch), so that the advection velocity is not easily estimated at small $\Delta t_{obs}$. The value $\Delta t_{obs} \approx 0.2$ days corresponds to the longest interval that can be used to estimate velocity without violating the CFL criterion. The values of the *Gain* for $\Delta t_{obs}$ of 1-2 days is of the order of 15-25% for the concentration and 20-25% for the velocity.

*4.2. The VAR experiments: sensitivity to flow variability*

The VAR experiments illustrate the dependence of the estimates on time and space variability of the flow field. Estimates for 20 different realizations (10 release locations and two flow fields) have been computed for a realistic value of $\Delta t_{obs} = 1$ day and for modalities $CC$ and $CB$. The results are summarized in Table 2 in terms of mean and standard deviation of the *Gain* for velocity and concentration, computed over all the realizations and daily values. As it can be seen, the mean values are similar for velocity and concentration, and range around 30-40% for $CC$ and 15% for $CB$. The standard deviations are quite high, approximately half of the mean for $CC$ and almost of the same order for $CB$. If we compare the mean values with the *Gain* values for the BASE experiment for $\Delta t_{obs} = 1$ day (Fig.5), we can see that the BASE values are higher than the means, but well inside the variability.

The high variability can be due to various factors. For the velocity, the main factor is likely the initial position of the patch within the velocity field in the Truth and in the Model. Since only the cross-component is corrected by the method, the *Gain* is expected to be high mainly when the

cross-component of the Truth and of the Model are significantly different. For the concentration, since the patch evolution depends only on the cross-component of the velocity, the main factors are expected to be the accuracy with which this component is estimated by (5), (which in turns depends on the estimates of the space and time derivatives (3)), and the pattern of advection between successive corrections, i.e. during $\Delta t_{obs}$. In particular, for $\Delta t_{obs}$ of the order of 1 day, if the estimated velocity has significant errors the patch can be partially advected in an area different from the True patch. When this happens, i.e. the estimated patch lies outside the True patch, there will be no significant correction at subsequent times and the patch will be lost, i.e. it will behave as if advected by the Model velocity only.

This effect is illustrated in the example shown in Fig.6, displaying concentration and velocities for Truth (upper panels), Model (upper middle panels) and Estimates for $CC$ and $CB$ (lower-middle and lower panels) after 3 days for a release location in the northwestern area, at point (15,13). The blue circles superimposed on the Truth and Model velocities indicate the initial patch release, while the red lines superimposed on the estimated velocities indicate the regions where the velocity correction is active at day 3, i.e. regions with concentration greater than the cutoff $c_{cutoff}$=0.1. The patterns of the patch at day 3 are significantly different in the Truth and in the Model. The Model patch is caught in a strong eastward jet, that advects it and elongates it toward the east. This jet is not present in the Truth, so that the patch does not move significantly and keeps closer to the northwestern corner. For the $CC$ estimate, a small part of the patch appears to have escaped eastwards, outside the red line indicating the correction region. This effect is even more

pronounced for $CB$, where the degradation in the velocity estimation causes the concentration to move with the Model velocity well outside the region of the True patch. This is reflected by the pattern of the estimated $CB$ concentration, that shows significant corrections with respect to the Model in the northwestern corner, while the eastern side is very similar to the Model one. A different example of release is shown in Fig.7. In this case, both the $CC$ and $CB$ modalities are able to maintain the estimated patch within the correction region. The overall correction is very effective, as can be seen comparing visually the estimated concentration and velocity fields with the Truth and Model ones, in particular for $CC$, as can be expected.

*4.3. The PATCH experiments: sensitivity to patch characteristics*

The PATCH experiments are performed similarly to the BASE experiments, but they consider different parameters characterizing the patch. In all cases, the same release location and the same velocity field as in BASE are used.

The first considered parameter is the cutoff value $c_{cutoff}$ used to define the patch in modality $CC$ and $CB$. In BASE the cutoff was set to $c_{cutoff}$=0.1, while here the value $c_{cutoff}$=0.35 is also considered. This corresponds to assuming that only higher intensities are detected by observations, so that only the core of the patch is observed, and the patch itself appears smaller ($c_{cutoff}$=0.35 approximately corresponds to the green contours in Fig.4). A set of experiments is performed in modality $CB$ varying $\Delta t_{obs}$ as in BASE. The results in terms of *Gain* are shown and compared with the BASE results in Fig. 8. The dashed (dotted) lines indicate the PATCH (BASE) results. As can be seen they are qualitatively similar, aside from some differences for

the concentration at small $\Delta t_{obs}$. Notice that the *Gain* metric is computed as for BASE, i.e. computing (8) in regions with $c_{cutoff} > 0.1$. If instead the *Gain* is computed using $c_{cutoff}$=0.35, then its values increase for the PATCH experiment (solid line), reaching approximately 35-40% for $\Delta t_{obs} = 1$ day for both concentration and velocity. These values are higher than the BASE values even if computed using $c_{cutoff}$=0.35 (not shown).

Overall, the results indicate that changing the cutoff value does not have a strong effect on the *Gain*, especially when computed over the extended patch. When the *Gain* is computed only on the core of the patch, an increase of approximately 15-20% is registered.

The second parameter that is varied is the size of the initial patch, i.e. the value of the Gaussian width $R$. In BASE, $R = 2\Delta s$, while here we also use $R = 1.2\Delta s$. Smaller sizes are not considered since they could lead to numerical problems in the integration of the advection equation (1). Experiments in the three modalities $CA$, $CC$ and $CB$ have been performed varying $\Delta t_{obs}$ as in BASE, and the *Gain* results are shown in Fig.9. The overall patterns are similar to the BASE results in Fig.5, aside from the fact that the $CB$ *Gain* for the concentration decreases abruptly for $\Delta t_{obs} > 1$ day, while it keeps relatively high for the velocity. We remark that the details of the curves depend on the specific release location considered, and therefore cannot be considered completely general. On the other hand, the effect appears sufficiently strong to suggest that it might be generally significant. A possible explanation for this result is that, since the patch is smaller, it is more prone to the effects described in Section 4.2. When $\Delta t_{obs}$ is long enough and the advection velocity is not perfectly estimated, the estimated patch might be

more easily lost, since the correction region is smaller. This would explain why the *Gain* for the concentration decreases abruptly for long $\Delta t_{obs}$, while the *Gain* for the velocity is maintained.

Finally, we consider the sensitivity to the details of the evolution of the patch. In BASE, the patch was advected integrating equation (1) using a third order upwind scheme. Here we consider a first order scheme, that is expected to be significantly more diffusive (Durran, 1999). For such a scheme the diffusivity can be estimated on the basis of the relationship (Kantha and Clayson, 2000):

$$K = \frac{1 - C_r}{2} C_r \frac{\Delta s^2}{\Delta t}, \tag{9}$$

where

$$C_r = U \frac{\Delta t}{\Delta s} \tag{10}$$

is the Courant number; for our parameters, $K$ results of the order 600 $m^2/s$, i.e. lower than, but not too far from, the mesoscale diffusivity drawn from drifter data in the Mediterranean ($1 \div 5\ 10^3 m^2/s$, with a typical value of $3\ 10^3 m^2/s$, see Falco et al., 2000; Gerin et al., 2007; Poulain and Zambianchi, 2007).

An example of the effects of higher diffusion is shown in Fig.10 where the tracer concentration at day 3 is depicted for the Truth (left panel) and the Model (right panel). A visual comparison with the corresponding BASE results in Fig.4 clearly indicates that, while the patterns are similar, the gradients are significantly smoother in PATCH (notice the scale difference

between Fig.4 and Fig.10 to accommodate the fact that the maximum concentration is significantly lower in presence of strong diffusion).

The same set of experiments as in BASE has been performed, varying $\Delta t_{obs}$ for $CA$, $CC$, $CB$. Conceptually, the comparison with the BASE results is expected to serve two purposes. On one hand, it will indicate whether or not there is a dependence of the results on the specific numerical scheme used for advection. On the other hand, a more physical interpretation of the results can be considered, indicating whether or not the method holds also in presence of strong diffusivity. Notice that in the PATCH experiments the strong diffusion is not directly considered in the estimation formulas (3) and (5), that are kept the same as in BASE, i.e. with $f = 0$. In this sense, the test corresponds to the realistic case where the estimate is performed assuming a simple advective process, while the patch actually evolves in a more complex way.

The results in terms of *Gain* for velocity and concentration are shown in Fig.11, and they can be compared with the BASE results in Fig.5. A good qualitative resemblance can be noticed, indicating that the method is robust and provides correct estimates even in cases when the dynamics of the patch is significantly different from pure advection. It is interesting to notice that in the presence of diffusion (Fig.11) the method appears stable also for $CA$ up to $\Delta t_{obs} \approx 1.5$ days, that is significantly higher than for BASE (Fig.5). This suggests that smoothing the gradients tends to eliminate the instability problems of the method, as can be expected.

## 5. Summary and concluding remarks

In this paper, a recently proposed method (Piterbarg, 2009) has been implemented and tested to estimate surface velocities in the ocean by fusing information from satellite tracer data and from velocity model outputs. The method is tested using synthetic data in the framework of the twin experiment approach, using realistic velocity outputs produced by the operational Mediterranean Forecasting System. The method is general and can include the fate of the tracer, i.e. its physical and chemical transformation. The configuration considered in this paper, though, is simple and corresponds to a patch of tracer passively advected by the surface current. It can be regarded as a first step towards approaching the practical problem of estimating the advection field and the evolution of the concentration of a pollutant released by a localized source, such as for instance an oil spill, using satellite data. The tracer is observed with a temporal resolution $\Delta t_{obs}$ and the data are used to correct the velocity field. The patch evolution is then recomputed using the estimated velocity, therefore improving the prediction of the tracer concentration.

An extensive set of tests has been carried out and the performance of the method has been quantified considering the improvement (*Gain*) of the estimated fields with respect to the model fields. In the ideal cases when concentration data are available over the whole region with a time resolution of the order of 1-2 hours, the *Gain* reaches values of 80-90% for the concentration and 50-60% for the velocity, which are close to the theoretical values for perfect data. In the more realistic cases of limited observations and longer $\Delta t_{obs}$ of the order of days, the *Gain* reduces. Various release loca-

tions and two different velocity configurations have been considered, and the mean *Gain* and its standard deviation have been computed for $\Delta t_{obs} = 1$ day. The variability is found to be quite high, depending primarily on the initial position of the patch within the velocity field, which in turns determines the relative size of the cross- and along-gradient components of velocity and the patch advective path during $\Delta t_{obs}$. The mean *Gain* for observations limited to high values of concentration inside the patch reaches values around 30-40% for both concentration and velocity. When only the boundary of the patch is observed, the *Gain* further reduces, even though it keeps significant, with values of 15-20% for velocity and concentration.

Further tests have been performed varying the parameters of the patch, such as width and concentration cutoff, and considering deviations from the purely advective evolution introducing a high numerical diffusivity, lower than, but not too far from, mesoscale diffusivity observed in the Mediterranean. In all these cases the results appear consistent, showing that the method is robust. In particular, the results with high diffusivity suggest that, even though the method is implemented assuming zero sources and sinks, results actually hold for cases that significantly deviate from these assumptions, such as possibly realistic cases where the patch might evolve in a complex way.

In summary, the experiments cover an extensive parameter space in terms of observation time intervals and modalities, as well as flow variability and patch parameters. The results are very encouraging, indicating the potential of the method for a number of practical applications. Oil spill detection from satellite is presently carried out using mainly synthetic aperture radar (SAR)

and/or optical sensors (for a recent review of different techniques see Brekke and Solberg, 2005). SAR sensors are currently hosted on a suite of different platforms (ERS2, RadarSAT1 and 2, Envisat, ALOS, TerraSAr and COSMO SkyMed); their revisit cycle is of the order of 3 days, but is expected to get down to 1 day or less - considering, in particular, the capabilities of reorienting the SAR instrument on COSMO SkyMed missions so as to get more frequent data coverage of a given region. Ocean color data utilizable for oil spill detection are presently provided by MODIS instruments onboard the EOS (Earth Observation Satellites) Terra and Aqua platforms, each offering daily global coverage, which may be complemented by the Medium Resolution Imaging Spectrometer (MERIS) on Envisat satellites, characterized by 2-3 day revisit time, thus potentially offering, all together, two passages a day during daytime in the case of clear sky conditions. The results of the present investigation suggest that for these realistic $\Delta t_{obs}$ a significant gain can be obtained in the estimation of velocity and concentration.

It is worth adding that satellites currently provide information only on the spill coverage, but there is ongoing research trying to identify also concentration levels inside the patch, in terms of oil thickness, at least from aircraft-mounted sensors (hyperspectral passive imagery and laser induced fluorescence are among the most suited ones, see, e.g., Lennon et al., 2006, rather than microwave sensors, discussed among the others by Fingas and Brown, 1997). Our results show that observations of tracer gradients inside the patch (modality $CC$) can lead to a significant improvement with respect to the observation of the boundary only (modality $CB$). Moreover, it is seen that in the $CC$ case decreasing $\Delta t_{obs}$ can lead to significant improvements.

We emphasize that the method is highly portable and computationally efficient, making it very valuable in the framework of operational strategies for rapid assessment and quick response. The present method has therefore some significant advantages with respect to other techniques requiring complete assimilation of the tracer information in the dynamical velocity models. These techniques, even though more powerful, require significant coding and computational time and they have to be set up in advance for the specific operational model in use.

The present results can be considered as an important first step in the investigation and application of the method. Future work is planned to generalize the present results in various directions. First of all, the present results specifically address the case of a tracer advected by mesoscale features. The issue of small scales in space and time is not considered here, and will be addressed in future works, still in the framework of the twin experiment approach, considering as Truth the results of a high resolution model in space and time. The presence of small scales will likely imply a pre-processing of the data, that will be smoothed at the scales of the Model in order to perform the estimation, as is common practice in many satellite data analysis applications (e.g., Reynolds et al., 2002; see also Rinaldi et al., 2009). A similar approach has been followed also for Lagrangian data assimilation in the presence of high frequency and small scale fluctuations (Taillandier et al., 2008). Another important point to consider is that the fate of the tracer is not considered in this application. A theoretical analysis of the impact of a partially unknown fate function for the estimation has been performed in Piterbarg (2009) and tested using ideal perfect data. A further investigation is needed considering

a more realistic setup to evaluate this effect for real data applications. Finally it is important to notice that the present results are obtained using the twin experiment approach. While the approach is very useful in providing quantitative skill assessment, it is intrinsically limited by the fact that the synthetic data are generated by models and therefore limited by the limitations of the models themselves. Applications to real data are the next, necessary step, and they will be carried out using historical oil spill data sets (see examples of comparisons between observations and models in Al-Rabeh et al., 1992; 2000) and using results from a dedicated recent experiment performed in the Mediterranean Sea in the framework of the PRIMI project (Santoleri et al., 2009). A realistic oil spill model for the Mediterranean Sea, MEDSLIK (http://www.oceanography.ucy.ac.cy/cycofos/medslik-act.html, Zodiatis et al., 2008), presently used as part of MFSTEP (Dombrowsky et al., 2009), will be included in the tests.

As a final remark, we notice that, while the present work is focused on the specific oil spill application, the method is general and future applications can be targeted also to sea surface temperature or ocean color data sets. For mesoscale applications, the requirements in terms of time and space sampling, as well as the necessary coverage in terms of tracer gradients, are expected to be similar to the ones considered in the present study. Different applications targeted to more climatic studies can also be envisioned, considering lower resolution data in space and time and smoother, general circulation velocity. The main challenge in this framework might come from the correct knowledge of the source and sink terms of the transport equation for the sea surface temperature and for ocean color derived tracer fields.

## 6. Acknowledgments

We gratefully acknowledge support from ASI (Agenzia Spaziale Italiana) PRIMI project (AM, AG, EZ), from ONR (Office Naval Research) grant N00014-09-1-0322 (LP) and grant N00014-05-1-0094/95 (AG), and from NSF (National Science Foundation) grant CMG-0530893 (LP). The authors have benefited from insightful conversations with R. Santoleri, F. Bignami and F. Nirchio on satellite applications and with G. Buffoni and N. Pinardi on modelling issues.

| Exp | $\mathbf{x}_0$ | R(in $\Delta s$ units) | $\Delta t_{obs}$(in days) | Obs. modality | $c_{cutoff}$ |
|---|---|---|---|---|---|
| BASE | 1 location | 2 | 0.01, 0.1, 0.2, 0.25, 0.5, 1.0, 1.5, 3.0 | $CA$, $CC$, $CB$ | 0.1 |
| VAR | 10 locations | 2 | 1 | $CB$, $CC$ | 0.1 |
| PATCH | 1 location | $1.2 \div 2.0$ every 0.1 | 0.01, 0.1, 0.2, 0.25, 0.5, 1.0, 1.5, 3.0 | $CA$, $CC$, $CB$ | 0.1, 0.35 |

Table 1: Characteristics and parameters of the different sets of numerical experiments (see Section 3.3 for definitions)

| | *Gain* **u** (%) | | *Gain* c (%) | |
|---|---|---|---|---|
| Observ. modality | mean | stand. dev. | mean | stand. dev. |
| $CC$ | 33 | 16 | 37 | 22 |
| $CB$ | 14 | 10 | 14 | 10 |

Table 2: Means and standard deviations of the *Gain* for velocity and concentration for the VAR experiments ($\Delta t_{obs}$=1 day)

**Figure Captions**

**Figure 1** : Schematic illustration of the fusion method for the model velocity estimate and tracer observations. Left panel: Multiple model output (red points) and a poorly known forcing. The shaded area shows a confidence region for the real velocity coming from tracer observations. Right panel: Single model output and an exactly known forcing. The estimate is obtained as projection of the model on the line.

**Figure 2** : Domain of the experiments (blue rectangle) with an example of MFS velocity output.

**Figure 3** : Map of release locations for the VAR experiments superimposed to the Truth velocity field used in the following figures.

**Figure 4** : BASE experiments. Right panels show the velocity field and left panels the patch tracer concentration at day 3 for the Truth (upper), Model (middle upper), Estimate in modality $CA$ and $\Delta t_{obs} = 0.1$ days (lower-middle) and $\Delta t_{obs} = 0.25$ days (lower). The blue circles superimposed on the velocity fields indicate the initial patch releases.

**Figure 5** : BASE experiments. Plots of $Gain$ versus $\Delta t_{obs}$ for velocity (upper panel) and concentration (lower panel). Blue lines indicate results obtained in modality $CA$, red lines in modality $CC$ and green lines in modality $CB$.

**Figure 6** : VAR experiments. Right panels show the velocity field and left panels the patch tracer concentration at day 3 for the Truth (upper), Model (middle upper), Estimate in modality $CC$ and $\Delta t_{obs} = 1$ day (lower-middle) and Estimate in modality $CB$ and $\Delta t_{obs} = 1$ day (lower). The blue circles superimposed on the velocity fields indicate the initial patch releases,

the red lines indicate the regions where the velocity correction is active at day 3, i.e. regions with concentration greater than the cutoff $c_{cutoff}$=0.1.

**Figure 7** : VAR experiments. Right panels show the velocity field and left panels the patch tracer concentration on day 3 for the Truth (upper), Model (middle upper), Estimate in modality $CC$ and $\Delta t_{obs} = 1$ day (lower-middle) and Estimate in modality $CB$ and $\Delta t_{obs} = 1$ day (lower). The blue circles superimposed on the velocity fields indicate the initial patch releases, the red lines indicate the regions where the velocity correction is active at day 3, i.e. regions with concentration greater than the cutoff $c_{cutoff}$=0.1.

**Figure 8** : PATCH experiments with $c_{cutoff}$=0.35 and modality $CB$. Plots of $Gain$ versus $\Delta t_{obs}$ for velocity (upper panel) and concentration (lower panel). Solid (dotted) lines indicate $Gain$ values computed in the region with concentration higher than 0.35 (0.1). Dashed lines show the BASE result for comparison, computed with $c_{cutoff}$=0.1.

**Figure 9** : PATCH experiments with $R = 1.2\Delta s$. Plots of $Gain$ versus $\Delta t_{obs}$ for velocity (upper panel) and concentration (lower panel). Blue lines indicate results obtained in modality $CA$, red lines in modality $CC$ and green lines in modality $CB$.

**Figure 10** : Example of a PATCH experiment with higher diffusivity. Patch tracer concentration at day 3 for the Truth (left) and Model (right).

**Figure 11** : PATCH experiments with higher diffusivity. Plots of $Gain$ versus $\Delta t_{obs}$ for velocity (upper panel) and concentration (lower panel). Blue lines indicate results obtained in modality $CA$, red lines in modality $CC$ and green lines in modality $CB$.

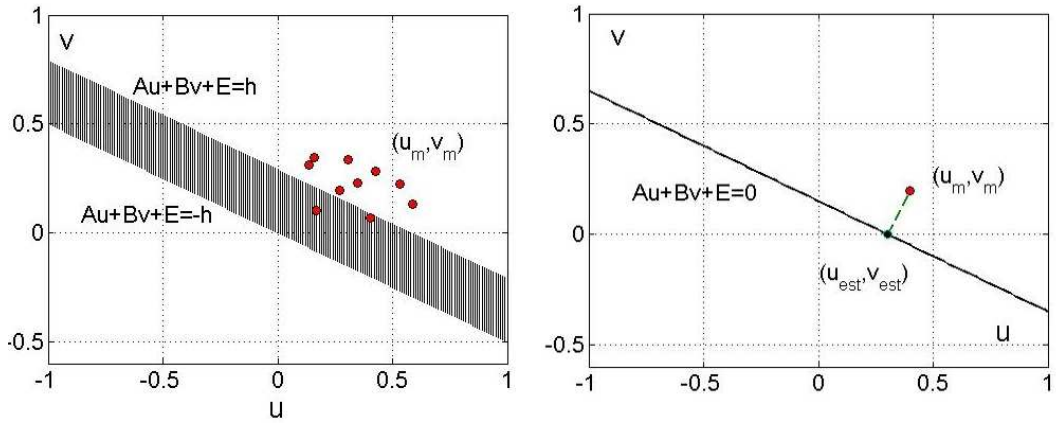


Figure 1:

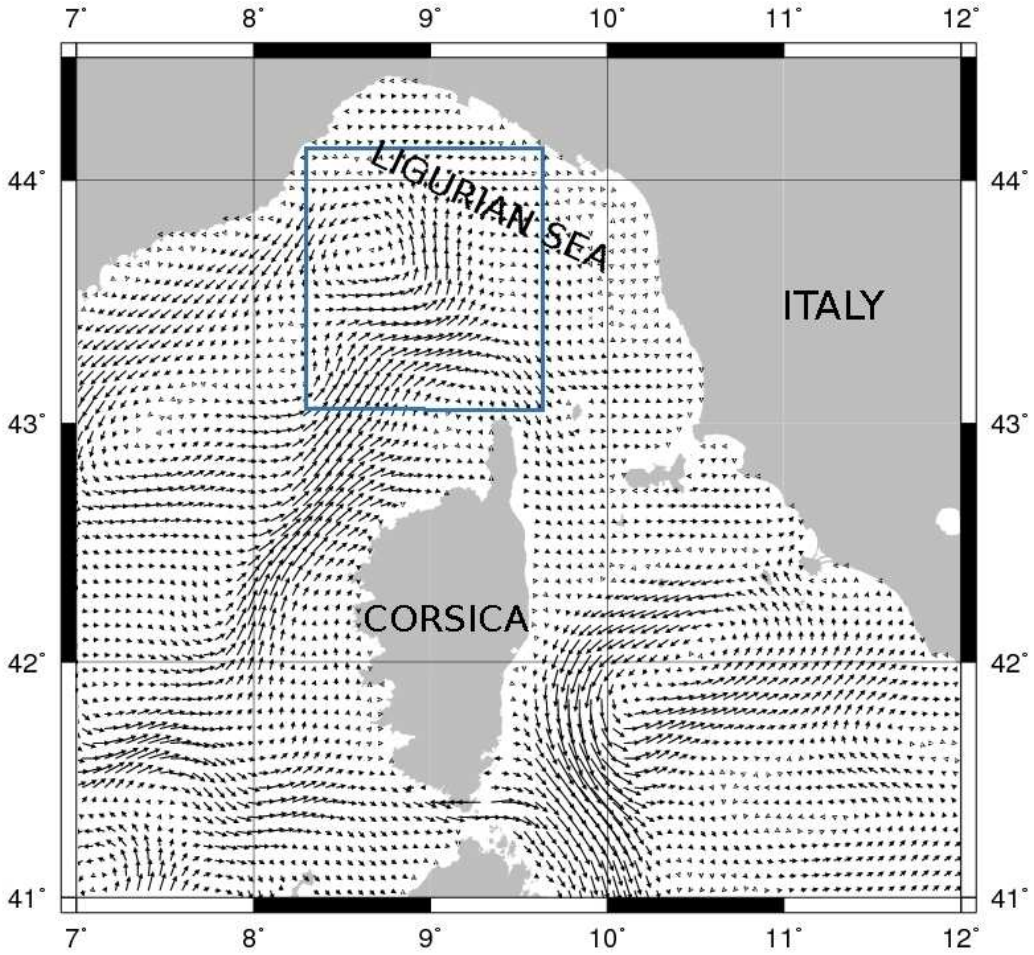


Figure 2:

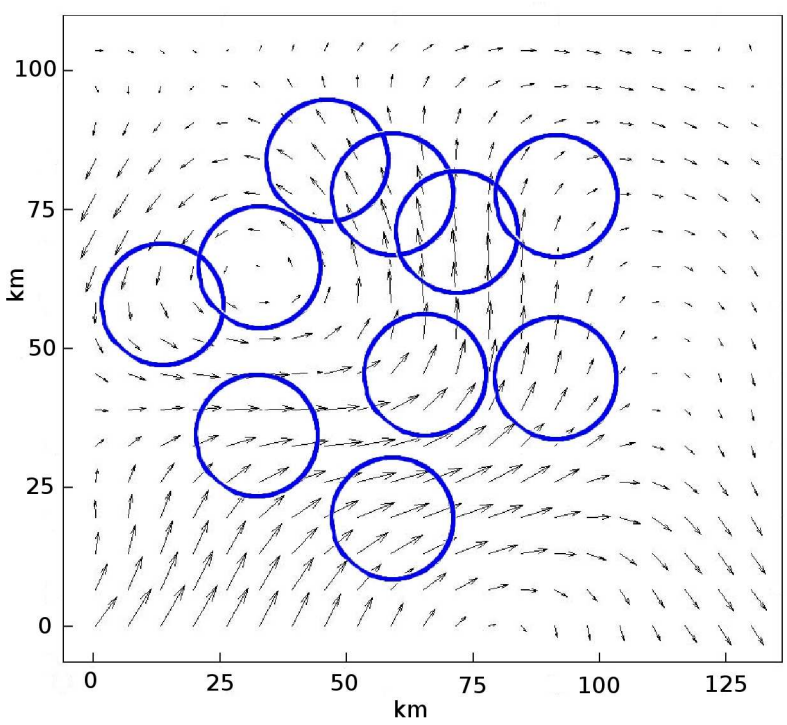


Figure 3:

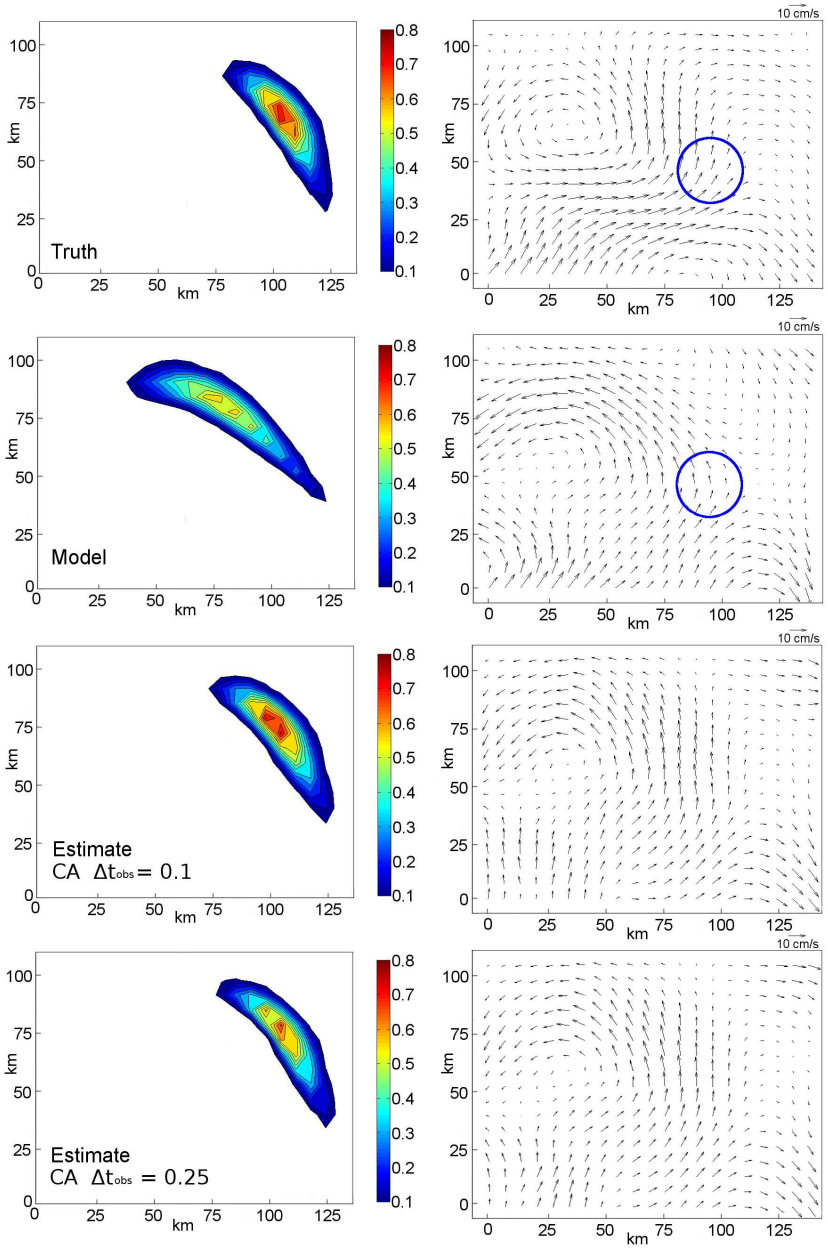
Truth
Model
Estimate
CA Δtobs = 0.1
Estimate
CA Δtobs = 0.25
km
10 cm/s

Figure 4:

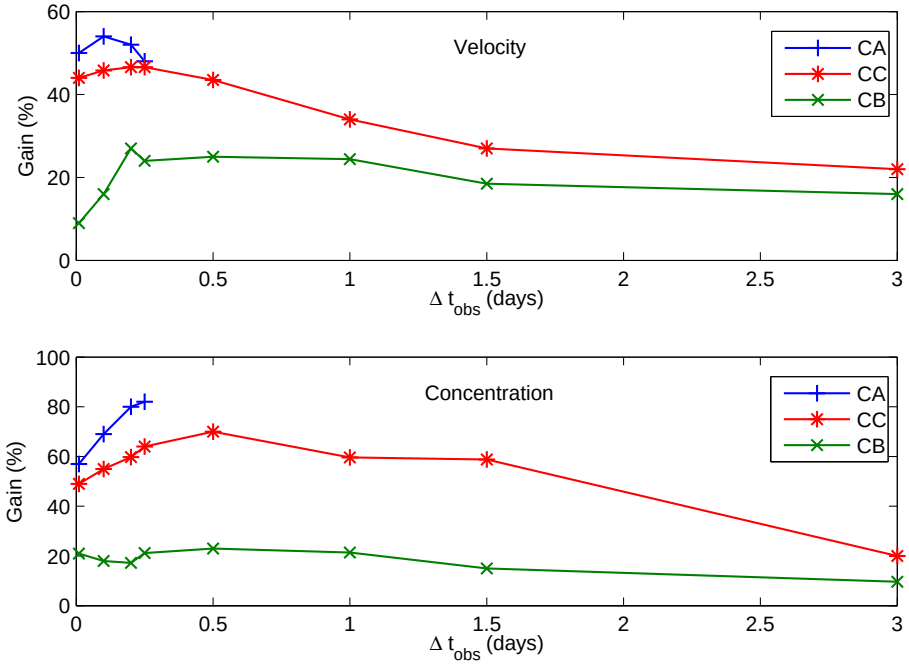
Velocity
CA
CC
CB
Gain (%)
Δ t obs (days)
Concentration
CA
CC
CB
Gain (%)
Δ t obs (days)

Figure 5:

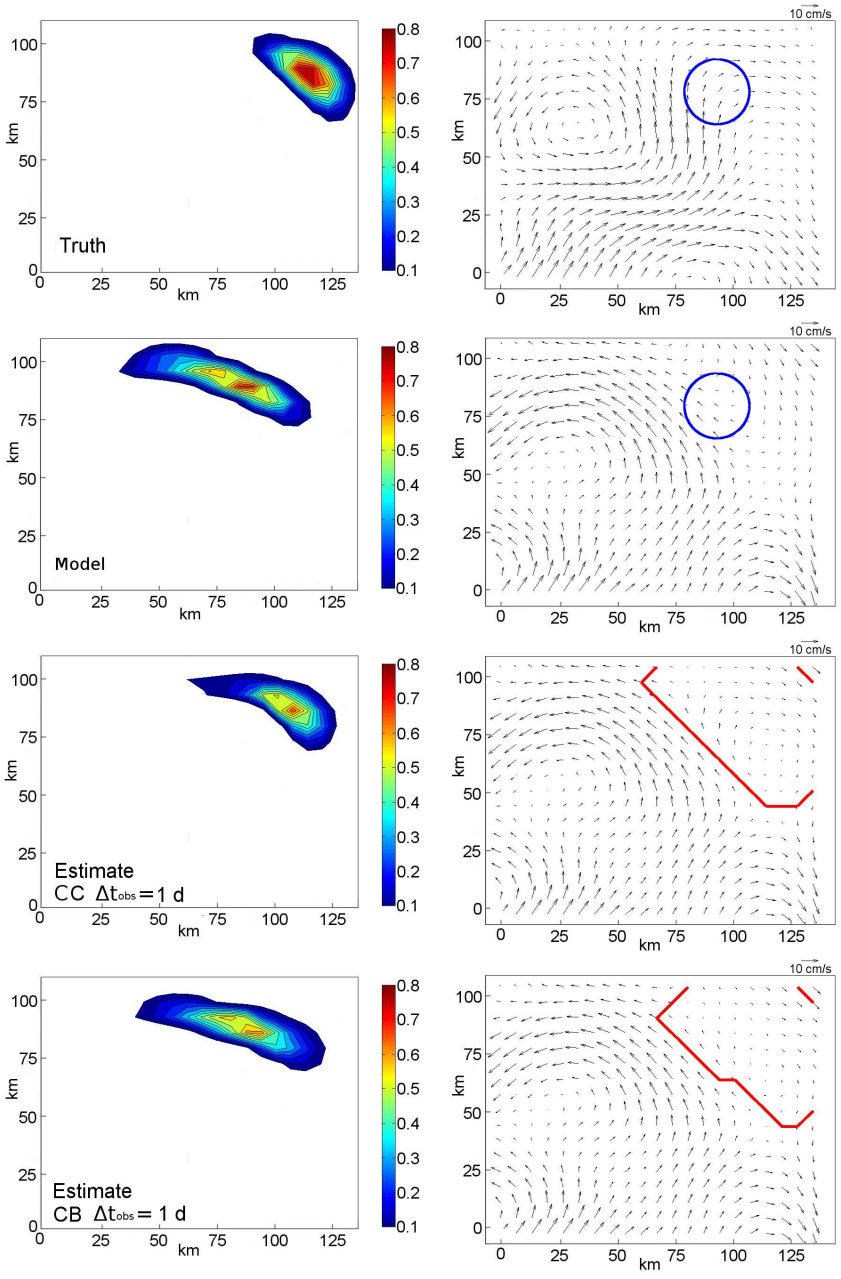
Truth
Model
Estimate
CC Δtobs = 1 d
Estimate
CB Δtobs = 1 d
km
10 cm/s

Figure 6:

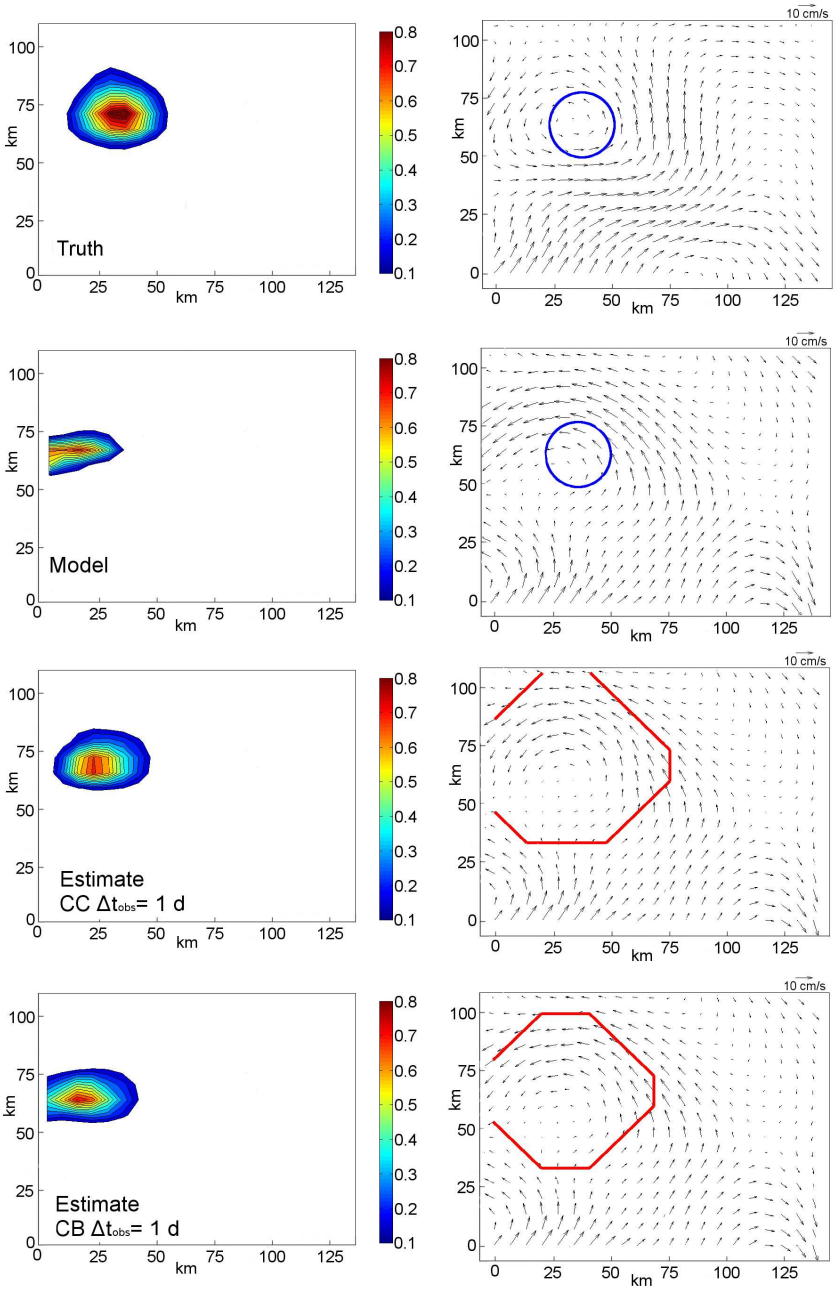
Truth
Model
Estimate
CC Δtobs= 1 d
Estimate
CB Δtobs= 1 d
km
10 cm/s

Figure 7:

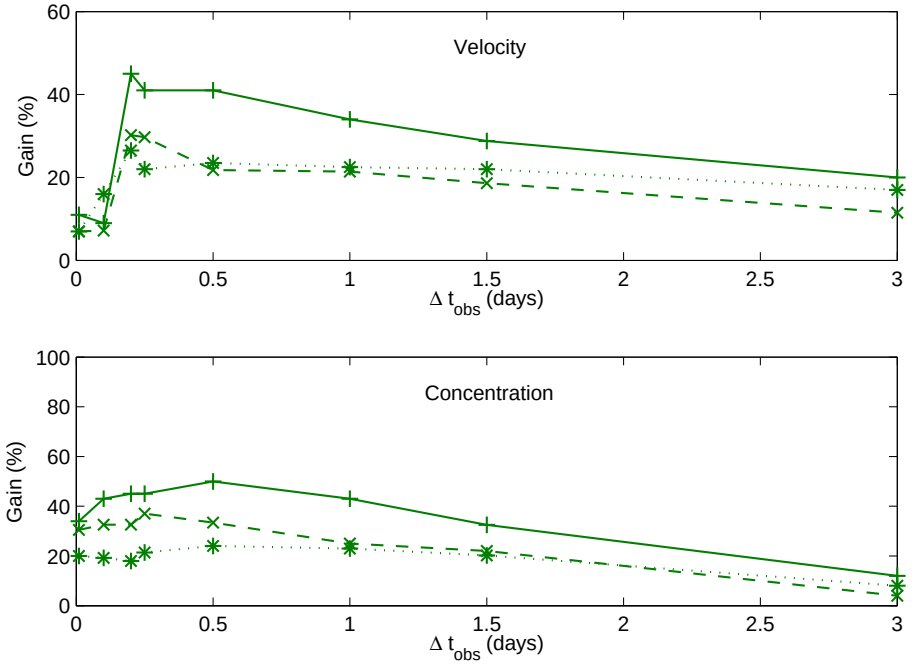


Figure 8:

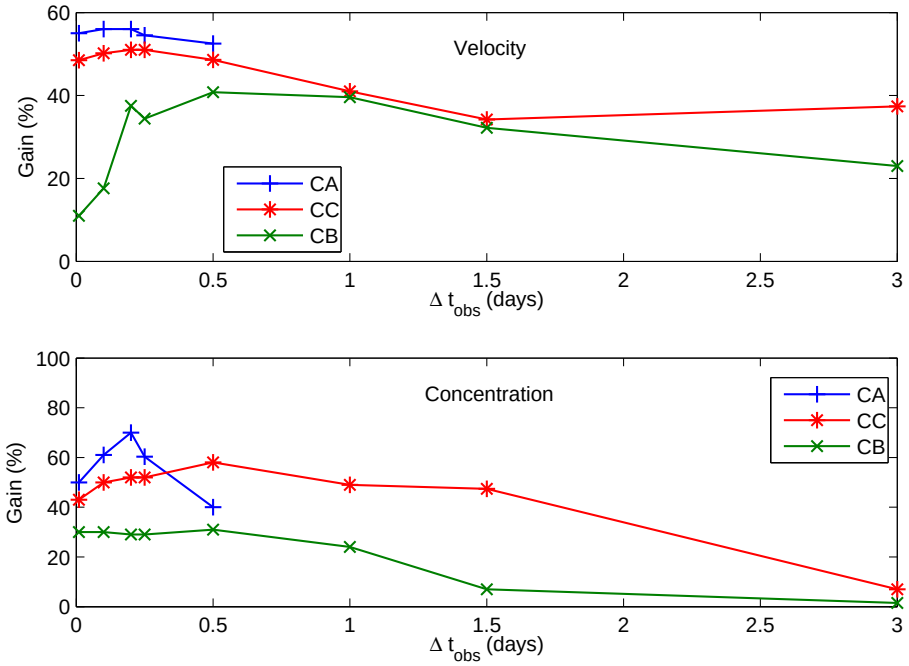


Figure 9:

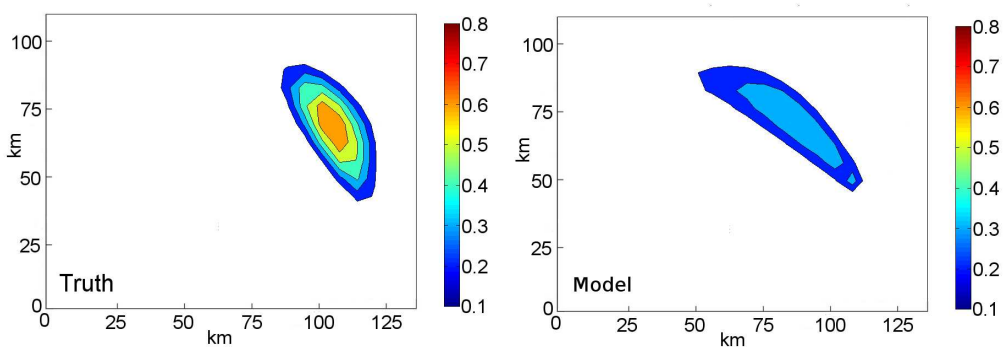


Figure 10:

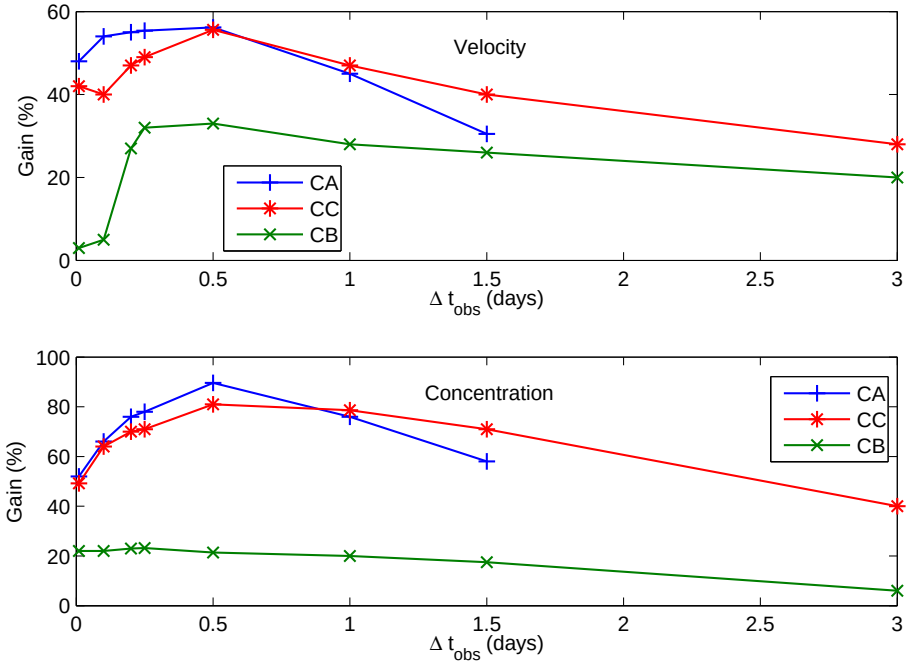
Velocity
Gain (%)
Δ t obs (days)
CA
CC
CB
Concentration
Gain (%)
Δ t obs (days)
CA
CC
CB

Figure 11:

## References


Al-Rabeh, A.H., Cekirge, H.M., Gunay, N., 1992. Modeling the fate and transport of the Al-Ahmadi spill. Water Air Soil Poll. 65, 257-279.

Al-Rabeh, A.H., Lardner, R.W., Gunay, N., 2000. Gulfspill Version 2.0: a software package for oil spills in the Arabian Gulf. Environ. Modell. Softw. 15 (4), 425-442.

Astraldi, M., Gasparini, G., Manzella, G., 1990. Temporal variability of currents in the Eastern Ligurian Sea. J. Geophys. Res. 95(C2), 1515-1522.

Bauer, S., M.S. Swenson, Griffa, A., 2002. Eddy-mean flow decomposition and eddy diffusivity estimates in the tropical Pacific Ocean. 2: Results. J. Geophys. Res., 107, (C10), 3154-3171.

Bennett, A.F., 1992. Inverse Methods in Physical Oceanography. Cambridge University Press, Cambridge MA.

Bereziat, D., Herlin, I., Younes, L., 2000. A generalized optical flow constraint and its physical interpretation. Proc. CVPR IEEE, 2, 487-492.

Brekke, C., Solberg, A.H.S., 2005. Oil spill detection by satellite remote sensing. Rem. Sens. Env. 95, 1-13.

Cohen, I., Herlin, I., 1996. Optical flow and phase portrait methods for environmental satellite image sequences, in: Buxton, B., Cipolla, R. (Eds), Computer Vision ECCV '96, Springer, Berlin. Vol. II, pp. 141-150.

Corpetti, T., Memin, E., Perez, P., 2002. Dense estimation of fluid flows. IEEE T. Pattern Anal. 24, 365-380.

Courant, R., Friedrichs, K., Lewy, H., 1928. ber die partiellen Differenzengleichungen der mathematischen Physik. Math. Ann. 100, 1, 32-74.

Crocker, I., Matthews, D., Emery, W.J., Baldwin, D., 2007. Computing Ocean Surface Currents from Infrared and Ocean Color Imagery. Trans. Geosci. Rem. Sens. vol. 45, n.2, 435-447.

Cuzol, A., Memin, E., 2005. Vortex and source particles for fluid motion estimation, in: Kimmel, R., Sochen, N., Weickert, J. (Eds), Scale Space and PDE Methods in Computer Vision, Springer, New York. pp. 254-266.

Dobricic, S., Pinardi, N., Adani, M., Bonazzi, A., Fratianni, C., Tonani, M., 2005. Mediterranean Forecasting System: An improved assimilation scheme for sea-level anomaly and its validation. Q. J. Roy. Meteor. Soc. 131, 3627-3642.

Dombrowsky, E., Bertino, L., Brassington, G., Chassignet, E., Davidson, F., Hurlburt, H., Kamachi, M., Lee, T., Martin, M., Mei, S., Tonani, M., 2009. GODAE systems in operation. Oceanography, 22 (3), 80-95.

Dubois, D., Prode, H., Yager, R.R. 1997. Fuzzy information engineering: a guided tour of applications. John Wiley & Sons, New York.

Durran, D.R., 1999. Numerical methods for wave equations in geophysical fluid dynamics. Springer, New York.

Emery, W.J., Fowler, C.W., Clayson, C.A., 1992. Satellite image derived Gulf Stream currents. J. Atmos. Ocean. Tech. 9, 285-304.

Emery, W.J., Thomas, A.C., Collins, M.J., Crawford, W.R., Mackas, D.L., 1986. An objective procedure to compute surface advective velocities from sequential infrared satellite images. J. Geophys. Res. 91, 12, 12865-12879.

Fabbroni, N., Pinardi, N., Oddo, P., DeMarte, M., Manzella, G., Poulain, P.M., Griffa, A., Torrisi, L., Lermusiaux, P., 2009a. Maritime Rapid Environmental Assessment Experiment in the Ligurian Sea, Part 1: Development of Relocatable Ocean Prediction System. In preparation.

Fabbroni, N., Pinardi, N., Oddo, P., DeMarte, M., Manzella, G., Poulain, P.M., Griffa, A., Torrisi, L., Lermusiaux, P., 2009b. Maritime Rapid Environmental Assessment Experiment in the Ligurian Sea, Part 2: Drifters trajectories simulation using Relocatable Ocean Prediction System. In preparation.

Falco, P., Griffa, A., Poulain, P., Zambianchi, E., 2000. Transport Properties in the Adriatic Sea as deduced from Drifter Data. J. Phys. Oceanogr. 30, 2055-2071.

Fiadeiro, M.E., Veronis, G., 1984. Obtaining velocities from tracer distributions. J. Phys. Oceanogr. 14, 1734-1746.

Fingas, M. F., Brown, C. E., 1997. Review of oil spill remote sensing. Spill Sci. Technol. B. 4, 199-208.

Frankignoul, C., Reynolds, R.W., 1983. Testing a dynamical model for mid-latitude sea surface temperature anomalies. J. Phys. Oceanogr. 13, 1131-1145.

Gerin, R., Poulain, P.-M., Taupier-Letage, I., Millot, C., Ben Ismail, S., Sammari, C., 2007. Surface circulation in the Eastern Mediterranean using Lagrangian drifters. Rapp. Comm. int. Mer Medit. 38.

Haynes, P.H., McIntyre, M.E., 1990. On the conservation and impermeability theorems for potential vorticity. J. Atmos. Sci. 47, 2021-2031.

Herlin, I., Le Dimet, F.X., Huot, E., Berroir, J.-P., 2004. Coupling models and data: which possibilities for remotely-sensed images?, in: Prastacos, P., Murillo, J. , Daz de Len, J.-L., Corts, U. (Eds), e-Environement: progress and challenges, Instituto Politcnico Nacional, Mxico, pp. 365-383.

Herlin, I., Huot, E., Berroir, J.P., Le Dimet, F.X., Korotaev, G., 2006. Estimation of a Motion Field on Satellite Images from a Simplified Ocean Circulation Model. IEEE Proceedings of the International Conference on Image Processing. 1077-1080.

Hernandez, F., Le Traon, P./Y., Morrow, R., 1995. Mapping mesoscale variability of the Azores Current using TOPEX/POSEIDON and ERS-1 altimetry, together with hydrographic and Lagrangian measurements, J. Geophys. Res. 100, 24995-25006.

Huot, E., Isambert, T., Herlin, I., Berroir, J.-P., Korotaev, G., 2006. Data assimilation of satellite images within an oceanographic circulation model. Int. Conf. Acoust. Spee. 2, 265-268.

Ide, K., Kuznetsov, L., Jones, C.K.R.T., 2002. Lagrangian data assimilation for point-vortex system. J. Turbulence, 3, 53-70.

Isambert, T., Berroir, J.P., Herlin, I., Huot, E., 2005. Apparent motion estimation for turbulent flows with vector spline interpolation. XVII IMACS world congress, Scientific Computation Applied Mathematics and Simulation. Paris, France, 11-15.

Kantha, L.H., Clayson, C.A., 2000. Numerical models of oceans and oceanic processes, Academic Press, San Diego.

Kelly, K.A., 1989. An inverse model for near-surface velocity from infrared images. J. Phys. Oceanogr. 19, 1845-1864

Korotaev, G.K., Huot, E., Le Dimet, F.-X., Herlin, I., Stanichn, S.V., Solovyev, D.M., Wu, L., 2008. Retrieving ocean surface current by 4-D variational assimilation of sea surface temperature images. Rem. Sens. Env. 112(4), 1464-1475.

Kurgansky, M.V., Budillon, G., Salusti, E., 2002. Tracers and potential vorticities in ocean dynamics. J. Phys. Oceanogr. 32, 3562-3577.

LaCasce, J.H., 2008. Statistics from Lagrangian observations. Progr. Oceanogr. 77, 1-29.

Lennon, M., Babichenko, S., Thomas, N., Mariette, V., Mercier, G., Lisin, A., 2006. Detection and mapping of oil slicks in the sea by combined use of hyperspectral imagery and laser induced fluorescence. EARSeL eProceedings. 5, 1-9.

Lumpkin, R., Treguier, A.-M., Speer, K., 2002. Lagrangian eddy scales in the northern Atlantic Ocean. J. Phys. Oceanogr. 32, 2425-2440.

Marshall, J., Olbers, D., Ross, H., Wolf-Gladrow, D., 1993. Potential Vorticity Constraints on the Dynamics and Hydrography of the Southern Ocean. J. Phys. Oceanogr. 23, 465-487.

Memin, E., Perez, P., 1998. A multigrid approach for hierarchical motion estimation. VI IEEE I. Conf. Comp. Vis. 933-938.

Molcard, A., Piterbarg, L.I., Griffa, A., Ozgokmen, T.M., Mariano, A.J., 2003. Assimilation of drifter positions for the reconstruction of the Eulerian circulation field. J. Geophys. Res. 108, 3056, doi:10.1029/2001/JC001240.

Needler, G.T., 1985. The absolute velocity as a function of conserved measurable quantities. Progr. Oceanogr. 14, 421-429.

Olbers, D.J., Wenzel, M., Willebrand, J., 1985. The inference of North Atlantic circulation patterns from climatological data. Rev. Geophys. 23, 313-356.

Ostrovskii, A.G., Piterbarg, L.I., 1995. Inversion for the heat anomaly transport from SST time series. J. Geophys. Res. 100, 4845-4865.

Ostrovskii, A.G., Piterbarg, L.I., 1997. A new method for obtaining velocity and mixing coefficients from time dependent distributions of tracer. J. Comput. Phys. 133, 340-360.

Ostrovskii, A.G., Piterbarg, L.I., 2000. Inversion of upper ocean temperature time series for entrainment, advection, and diffusivity. J. Phys. Oceanogr. 72, 301-315.

Papadakis, N., Memin, E., Cao, F., 2005. A variational approach for object contour tracking, in: Paragios, N., Faugeras, O., Chan, T., Schnorr, C. (Eds), Variational, geometric, and level set methods in computer vision, Springer, New York, pp. 259-270.

Piterbarg, L.I., 2009. A simple method for computing velocities from tracer observations and a model output. Appl. Math. Model. 33, 3693-3704

Poulain, P.-M. and Zambianchi, E., 2007. Near-surface circulation in the central Mediterranean Sea as deduced from Lagrangian drifters in the 1990's. Cont. Shelf Res. 27(7), 981-1001.

Reynolds, R.W., Rayner, N.A., Smith, T.M., Stokes, D.C., Wang, W., 2002. An improved in situ and satellite SST analysis for climate. J. Climate. 15, 1609-1625.

Rinaldi, E., Buongiorno Nardelli, B., Zambianchi, E., Santoleri, R., Poulain, P.-M., 2009. Lagrangian and Eulerian observations of the surface circulation in the Tyrrhenian Sea. J. Geophys. Res., doi:10.1029/2009/JC005535, in press.

Salman, H., Kuznetsov, L., Jones, C.K.R.T., Ide, K., 2006. A Method for Assimilating Lagrangian Data into a Shallow-Water-Equation Ocean Model. Mon. Weather Rev. 134(4), 1081-1101.

Santoleri, R., and the PRIMI group, 2009. The PRIMI cruise 2009: an innovative multiplatform oil spill experiment. In preparation.

Stommel, H., Schott, F., 1977. The beta spiral and the determination of the

absolute velocity field from hydrographic station data. Deep-Sea Res. 24, 325-29.

Taillandier, V., Griffa, A., 2006. Implementation of position assimilation from Argo floats in a realistic Mediterranean Sea model and twin experiment testing. Ocean Sci. 2, 223-236.

Taillandier, V., Griffa, A., Molcard, A., 2006. A variational approach for the reconstruction of regional scale Eulerian velocity fields from Lagrangian data. Ocean Model. 13(1), 1-24.

Taillandier, V., Griffa, A., Poulain, P.-M., Beranger, K., 2006b. Assimilation of Argo float positions in the north western Mediterranean Sea and impact on ocean circulation simulations. Geophys. Res. Lett. 33, L11604, doi:10.1029/2005GL025552.

Taillandier, V., Griffa, A., Poulain, P.M., Signell, R., Chiggiato, J.,Carniel, S., 2008. Variational analysis of drifter positions and model outputs for the reconstruction of surface currents in the Central Adriatic during fall 2002. J. Geophys. Res. 113, C04004, doi.1029/2007/JC004148.

Tonani, M., Pinardi, N., Dobricic, S., Pujol, I., Fratianni C., 2008. A high resolution free surface model of the Mediterranean Sea. Ocean Sci. 4, 1-14.

Turiel, A., Sol, J., Nieves, V., Ballabrera-Poy, J., Garcia-Ladona, E., 2008. Tracking oceanic currents by singularity analysis of Microwave Sea Surface Temperature images. Rem. Sens. Env. 112 , 2246-2260.

Vigan, X., Provost, C., Bleck, R., Courtier, P., 2000. Sea surface velocities

from Sea Surface Temperature image sequences. J. Geophys. Res. 105, 19499-19514.

Wunsch, C., 1977. Determining the general circulation of the ocean. A preliminary discussion. Science. 196, 871-875.

Wunsch, C., 1978. The North Atlantic general circulation west of 50 0 west determined by inverse methods. Rev Geophys. and Space Phys. 16, 583-620.

Zodiatis, G., Lardner R., Hayes, D.R., Georgiou, G., Sofianos, S., Skliris, N., Lascaratos, A., 2008. Operational ocean forecasting in the Eastern Mediterranean: implementation and evaluation. Ocean Sci. 4, 31-47.